Materials Horizons

REVIEW

View Article Online
View Journal | View Issue

Cite this: *Mater. Horiz.*, 2018, 5, 206

The progress and prospects of non-fullerene acceptors in ternary blend organic solar cells

Weidong Xu [ab] and Feng Gao [*a]

Received 12th November 2017,
Accepted 29th January 2018

DOI: 10.1039/c7mh00958e

rsc.li/materials-horizons

The rapid development of organic solar cells (OSCs) based on non-fullerene acceptors has attracted increasing attention during the past few years, with a record power conversion efficiency of over 13% in a binary bulk heterojunction architecture. This exciting development also enables new possibilities for ternary OSCs to further enhance their efficiency and stability. This review summarizes very recent developments of ternary OSCs, with a focus on blends involving non-fullerene acceptors. We also highlight the challenges and perspectives for further development of ternary blend organic solar cells.

1. Introduction

Organic solar cells (OSCs) are emerging as a promising candidate for delivering high efficiency at low manufacturing cost. A range of advantages, such as their non-toxicity and lightweight physical characteristics and the lucrative possibility of integration into flexible, semi-transparent, and colourful modules, enables various applications that may not be achievable in other thin film photovoltaic technologies.[1–16]

High performance OSCs are commonly fabricated with a bulk heterojunction (BHJ) structure, where one-donor and one-acceptor materials are blended to form a bi-continuous interpenetrating network with large interfacial area for exciton splitting.[17–24] Since organic semiconductors generally show low charge carrier mobility, the active layer usually has to be very thin (~100 nm) to ensure efficient charge collection. Such a thin film leads to limited light absorption and hence limited photocurrent. To address this issue, various strategies have been explored. For example, tandem cells which consist of multiple sub-cells with complementary absorption have been introduced, but the fabrication cost also significantly increases due to the complexity of preparing these devices.[25–27]

Alternatively, ternary blend OSCs featuring multiple light-harvesting materials in one active layer have emerged as one of the most promising strategies to improve photovoltaic performance.[28–34]

[a] *Department of Physics, Chemistry and Biology (IFM), Linköping University, Linköping 58183, Sweden. E-mail: fenga@ifm.liu.se*
[b] *Key Laboratory of Flexible Electronics (KLOFE) & Institute of Advanced Materials (IAM), Nanjing Tech University (NanjingTech), 30 South Puzhu Road, Nanjing 211800, China*

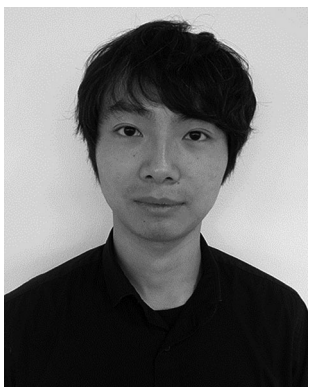

Weidong Xu

Weidong Xu received his BSc degree in Fine Chemistry from East China University of Science and Technology (China) in 2010. He obtained his PhD degree in Materials Science from the Institute of Advanced Materials (IAM) of Nanjing University of Posts and Telecommunications (China) in 2016. Later, he moved to Nanjing Tech University for postdoctoral research. Now he is a postdoc in the Department of Physics, Chemistry and Biology (IFM) at Linköping University (Sweden), working on organic applications.

Feng Gao

Feng Gao is an Associate Professor and a Wallenberg Academy Fellow at Linköping University in Sweden. He received his PhD from the University of Cambridge (UK) in 2011, followed by a Marie Curie postdoctoral fellowship at Linköping University. His group currently focuses on research into solution-processed energy materials and devices, mainly based on semiconducting polymers and metal halide perovskites.

Ternary blends possess the advantages of improving the photon harvesting ability as in tandem cells, while maintaining the straightforward fabrication that is utilized in single-junction devices. These advantages raise increasing interest in developing ternary solar cells with various compositions.[35–39] A typical ternary blend solar cell contains one additional electron donor or acceptor compared with its binary counterpart, and the third component is commonly selected to complement or extend the absorption scope of its binary host. Rationally selecting the third component and tuning the blend composition allow enhancing the light harvesting ability of the active layer and thus increasing the overall short circuit current density (J_{SC}). In addition, the third component might also be able to improve the charge transport, film morphology (polymer crystallinity, crystal orientation, domain size and purity), and exciton dissociation, leading to an enhancement of the fill factor (FF) and open-circuit voltage (V_{OC}).[28–35]

In fullerene-based ternary OSCs, incomplete light absorption is still a critical issue, considering that fullerene derivatives show very weak absorption in the abundant region of the solar spectrum. Very recently, non-fullerene acceptors (NFAs), which have already exhibited better photovoltaic performance than fullerene derivatives, have been developing rapidly.[40–42] For example, a high power conversion efficiency (PCE) of over 13% was reported very recently for fullerene-free binary blend OSCs.[43] With the rapid progress of high performance NFAs, their applications in ternary OSCs have been attracting more and more attention.[44] It is notable that a NFA based ternary OSC with a high efficiency of up to 14% has recently been demonstrated.[45]

Herein, we summarize recent developments of ternary OSCs based on NFAs. A brief introduction about the fundamental working mechanisms of ternary OSCs is presented, followed by discussions on the advantages of NFAs in ternary OSCs. Based on different material combinations, ternary OSC systems can be mainly classified into D–2A (one donor and two acceptors) and 2D–A (two donors and one acceptor) systems, which are discussed respectively. We emphasize the critical roles of NFAs in ternary blends, such as improving light absorption, tuning the morphology of the active layer, decreasing voltage loss, and improving device stability. Finally, we provide perspectives for future developments in this exciting research area.

2. Fundamental operating mechanisms and morphology models for ternary OSCs

In general, there are two operating mechanisms for the third component in ternary blends, *i.e.* charge transfer mechanism and energy transfer mechanism (Fig. 1).[46] The charge transfer mechanism is characterized by providing additional charge transport pathways for exciton dissociation and transport by adding the third component. One typical strategy based on this mechanism is to construct a cascade-like energy level alignment, as illustrated in Fig. 1a, where acceptor 1 serves as a bridge to transfer holes to the donor and deliver electrons to acceptor 2.

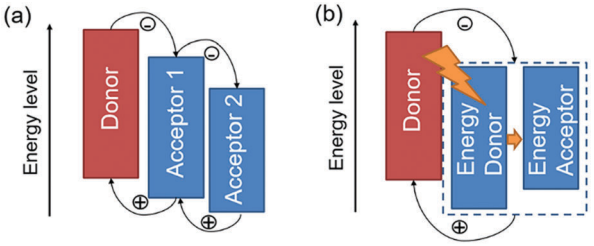

Fig. 1 The illustrations of the operating mechanisms of ternary OSCs with two different non-fullerene acceptors. (a) The charge transfer mechanism, where there is a cascade charge transfer alignment. (b) The energy transfer mechanism, where energy transfer occurs between two non-fullerene acceptors. The arrows indicate the charge transfer pathways. The lightning bolt in (b) illustrates an energy transfer process from one electron acceptor (energy donor) to the other (energy acceptor).

In addition, the energy transfer mechanism in ternary OSCs is an effective way to improve the light harvesting ability. In most of the energy transfer involved ternary OSC systems, a non-radiative fluorescence resonance energy transfer (Förster energy transfer, FRET) occurs among all three components or two of them. It requires overlapping between the photoluminescence (PL) of the energy donor and the absorption band of the energy acceptor. Fig. 1b exhibits an energy transfer process occurring between two non-fullerene acceptors. In fact, both charge transfer and energy transfer operating mechanisms can be intertwined in one ternary blend system.

It is proposed that the operating mechanism of the third component in a specific sample is strongly dependent on the morphology variation after the additional component loading. It has been revealed that the third compound can mix with one of the host materials or form its own phase.[47] In order to explain the difference, parallel-linkage and alloy models are proposed.[48] The morphological feature and charge transfer mechanism are depicted with the parallel-like model in Fig. 2a. Owing to the formation of independent donor/acceptor networks, there is no charge transfer or energy transfer between the two electron acceptors. Efficient charge transfer pathways form at either the donor/acceptor 1 or donor/acceptor 2 interface. This means that these ternary solar cells work like two individual sub-cells. In contrast, the alloy model requires an intimate mixing of two materials, forming the same frontier orbital energy levels, which are determined by the blend composition. As shown in Fig. 2b, the acceptor alloy works as a single material to extract electrons and deliver holes. In addition, due to good compatibility between the two materials, energy transfer also possibly occurs in the acceptor alloy if there is good spectral overlapping.

3. Advantages and functions of NFAs in ternary blend systems

3.1 Tunable absorption

The basic concept of ternary OSCs involves using an additional component to extend or increase the light absorption of

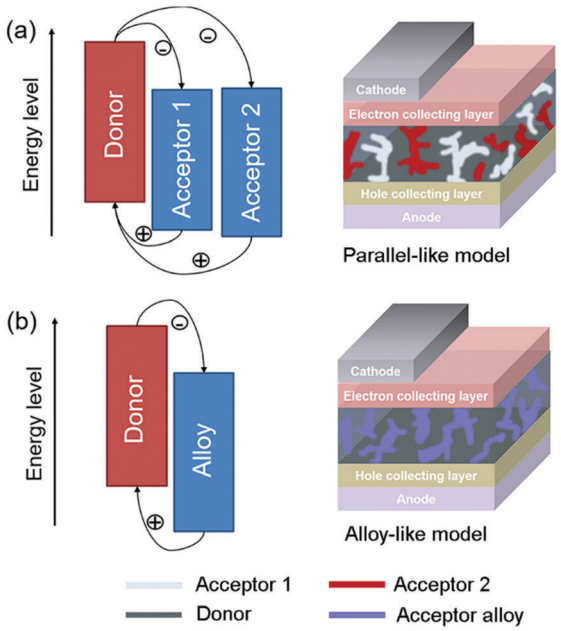

Fig. 2 The diagrams for proposed morphology models and related charge transfer processes in ternary OSCs with two different non-fullerene acceptors: (a) parallel-like model and (b) alloy-like model. The arrows indicate the charge transfer pathways.

the active layer. Therefore, a straightforward design rule is to introduce a third compound whose absorption complements its binary host. P-type conjugated polymers and small molecules, as well as dye materials, have all been introduced into ternary OSCs.[28–34] Considering the poor light harvesting ability of fullerene derivatives in the visible region, they are not favorable materials as the third component from the perspective of improving light absorption.

Introducing NFAs into ternary OSCs allows improving optical absorptivity due to their versatile chemical structures. Recently developed NFAs show much intense and broad absorption bands, which not only cover the whole visible region, but also extend to the NIR region up to 1000 nm, as shown in Fig. 3.[48–51] It is clearly advantageous for achieving more efficient solar cells due to the improved utilization of solar photons compared to fullerene derivatives. A blend film with three excellent light absorbers can provide flexible options to achieve complete light absorption across the whole abundant region of solar energy. Very recently, a large J_{SC} value exceeding 25 mA cm^{-2} was demonstrated in NFA ternary OSCs with a blend of PTB7-Th and J52 (Scheme 3) as the donor materials and a low band gap small molecule, IEICO-4F (Scheme 1), as the electron acceptor.[50] The external quantum efficiency (EQE) response for the ternary device crosses a large wavelength range from 300 nm to 1000 nm, indicating sufficient utilization of solar photons. In addition, the excellent light absorbing properties of NFAs provide a great opportunity to explore D–2A ternary systems, which have already become one of the hottest topics in the OSC research community. A very recent breakthrough demonstrated a high PCE value reaching 14% in a D–2A ternary system.[45]

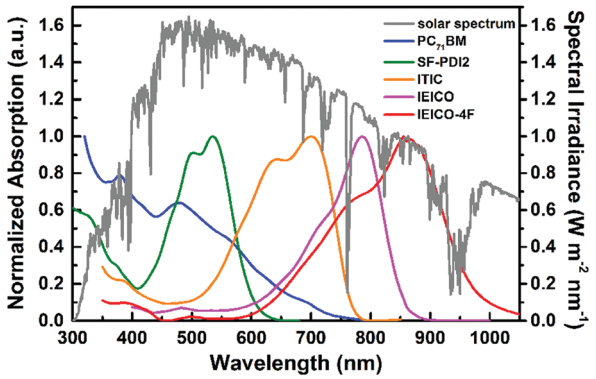

Fig. 3 Solar spectrum (global tilt) and normalized absorption spectra of typical electron acceptors (PC$_{71}$BM, SF-PDI2, ITIC, IEICO, IEICO-4F).[48–51] The chemical structures for the non-fullerene acceptors are shown in Schemes 1 and 2.

3.2 Small voltage loss and large V_{OC}

The voltage loss (ΔV) in solar cells is defined as the difference between the band gap of absorbers and the device V_{OC}. The voltage loss in solar cells can be attributed to the three factors as shown in the following equation:[52]

$$q\Delta V = (E_g - qV_{OC}) = (E_g - qV_{OC,SQ}) + (qV_{OC,SQ} - qV_{OC,rad}) + (qV_{OC,SQ} - qV_{OC}) = (E_g - qV_{OC,SQ}) + q\Delta V_{OC,rad} + q\Delta V_{OC,non\text{-}rad} = q\Delta V_1 + q\Delta V_2 + q\Delta V_3 \quad (1)$$

where q is the elementary charge, E_g is the bandgap of the photoactive material, $V_{OC,SQ}$ is the maximum voltage by the Shockley–Queisser limit. The first term of this equation (ΔV_1) is a result of radiative recombination loss above the bandgap of the active layer. This loss is unavoidable and its value is around 0.25–0.30 V. The second type of voltage loss (ΔV_2) is caused by the radiative recombination from the absorption below the bandgap due to sub-gap absorption, such as charge-transfer (CT) states or defect states.[53–58] The third part (ΔV_3) is assigned to any type of recombination event that is non-radiative, for example trap-assisted recombination. Both ΔV_2 and ΔV_3 are detrimental to photovoltaic performance and should be minimised.

Fullerene-based OSCs often suffer from large voltage losses. For example, poly(3-hexylthiophene)-2,5-diyl/[6,6]-phenyl-C61-butyric acid methyl ester (P3HT/PC$_{61}$BM) based devices show voltage losses around 1.35 V, while for the high performance PTB7 (Scheme 3)/[6,6]-phenyl C71 butyric acid methyl ester (PC$_{71}$BM) system, the value is around 0.87 V. In comparison, inorganic photovoltaic devices, such as c-Si and halide perovskite solar cells, generally exhibit small voltage losses around 0.40–0.55 V.[59–61] The large voltage loss for OSCs can be attributed to the requirement of a large energy level offset between the donor and acceptor for charge separation, CT states, and strong non-radiative recombination (ΔV_2 and ΔV_3 in eqn (1)). The energy level offset is believed to be the driving force for exciton dissociation. The way to reduce the energy level offset is either to downshift the highest occupied molecular orbital (HOMO)

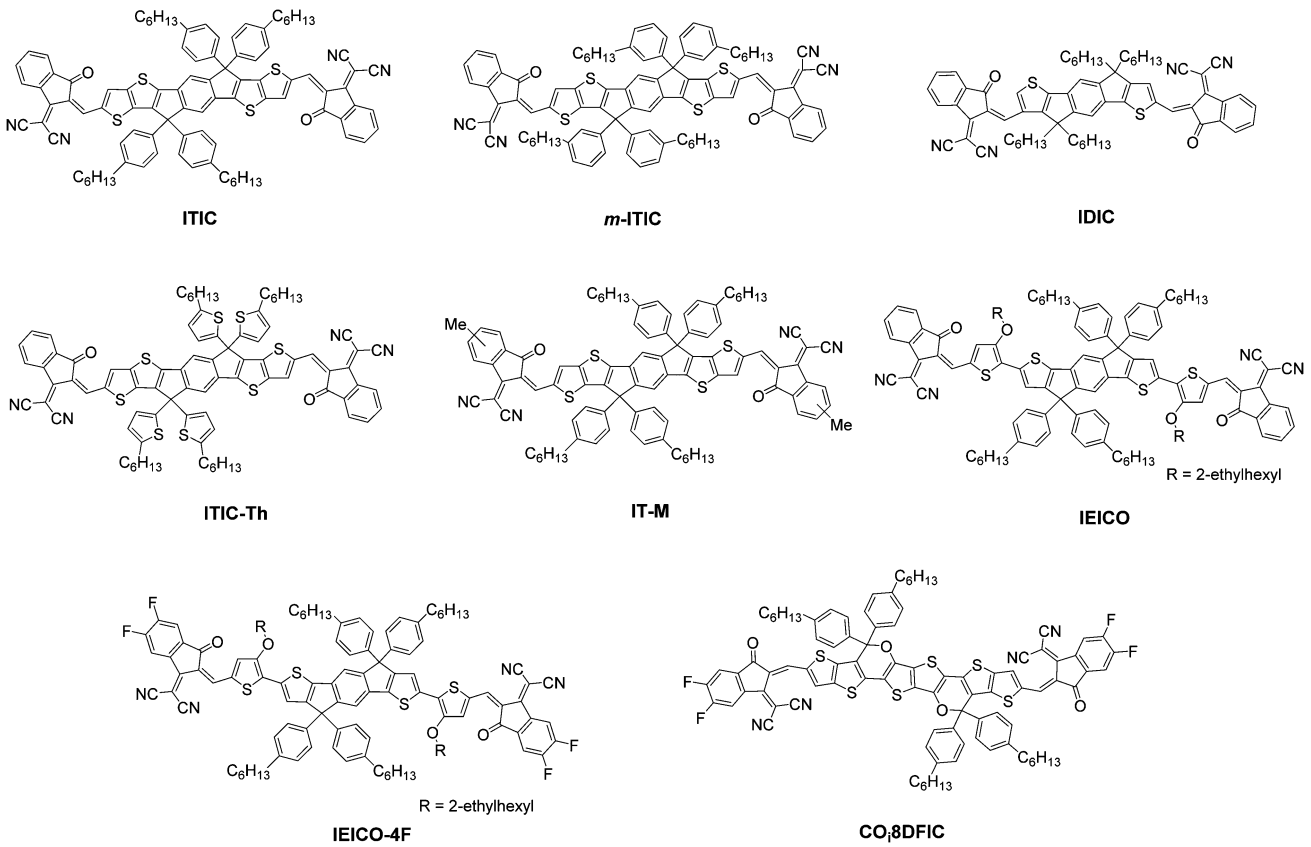

Scheme 1 The molecular structures of 2-(3-oxo-2,3-dihydroinden-1-ylidene)malononitrile (IC) based NFAs discussed in this review.

level of the donor or to upshift the LUMO level of the acceptor *via* molecular engineering. There have been several attempts to decrease this energetic difference in fullerene based OSCs. However, most of these attempts resulted in a significant photocurrent decrease and hence efficiency loss.[62–67] This indicates that there is a J_{SC}–V_{OC} trade-off in fullerene based OSCs.

For fullerene free OSCs, recent reports indicate that efficient and fast charge separation can be still achieved with a small driving force (less than 0.1 eV), for example in the blends of P3TEA and SF-PDI (Scheme 2).[52] As demonstrated by Fourier-transform photocurrent spectroscopy external quantum efficiency (FTPS-EQE) spectra (Fig. 4a), the overlap of the absorption onsets for pure P3TEA and P3TEA/SF-PDI (blend A) indicates that there is no sub-gap CT state absorption in blend films.[68] The small energy offset does not lead to any problematic issue in exciton dissociation, as suggested by a fast charge separation with a characteristic half lifetime of 3 ps. In addition, this system also exhibited a high EQE_{EL} value of 0.5×10^{-4}, representing a small non-radiative recombination voltage loss of 0.26 V. Its electroluminescence (EL) spectrum is nearly identical to that of the pure polymer device (Fig. 4b), indicating negligible emission from the CT states. With the combination of a small driving force and reduced non-radiative recombination, the voltage loss in this system was minimized to 0.61 V. Although it is possible that a small driving force could also be efficient in separating excitons in fullerene based solar cells, the very limited successful examples indicate that, at least, it is a very challenging task. For NFAs, their versatile structures and optoelectronic properties provide flexible options to achieve energy level alignment. It is also possible to reduce non-radiative V_{OC} loss through rational molecular design. The utilization of NFAs successfully decreases the V_{OC} loss with respect to fullerene based solar cells.[69]

In ternary blend OSCs, the V_{OC} is strongly dependent on their blend composition. The correlation between the V_{OC} and blend composition can be explained using the parallel-like model and alloy model.[70–73] In most cases, the V_{OC} is assumed to be a value between those obtained by the respective binary cells, and it can be continuously tuned by changing the feed ratio. This provides an opportunity for achieving more efficient solar cells by adding a third compound to increase the V_{OC} with respect to its major binary host, which has been widely demonstrated in fullerene based ternary OSCs.[70–73] Considering the small voltage loss of NFA based binary OSCs, the applications in ternary OSCs to enhance the V_{OC} are even more promising. In addition, recent work indicates that it is possible to obtain a V_{OC} which is even larger than both binary devices when NFA is utilized as the third component. Wang *et al.* reported a ternary blend system with $PC_{71}BM$/*m*-ITIC (Scheme 1) as the acceptor alloy.[74] By introducing a small amount of *m*-ITIC into the PTB7-Th:$PC_{71}BM$ host, the J_{SC} and V_{OC} increased significantly.

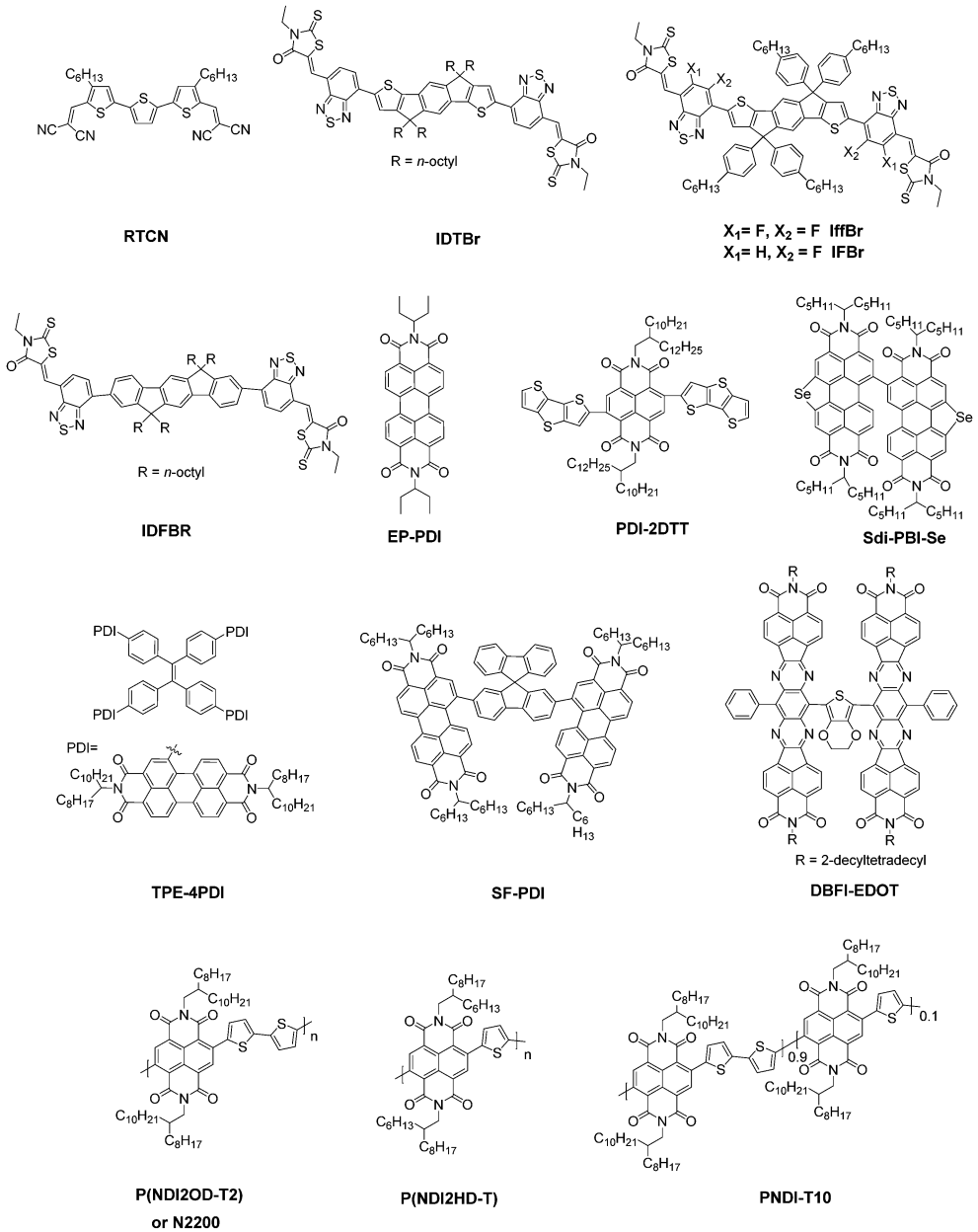

Scheme 2 The molecular structures of NFAs discussed in this review.

Both the V_{OC} and PCE peaked at a blend ratio of 1 : 1.05 : 0.45 (PTB7-Th : $PC_{71}BM$: *m*-ITIC). The maximum V_{OC} value was up to 0.854 V, which was 36 mV and 47 mV larger than those of the PTB7-Th:$PC_{71}BM$ and PTB7-Th:*m*-ITIC binary counterparts, respectively. The authors attributed the enhanced V_{OC} value to the cascade energy level alignment, which improved the exciton dissociation, and decreased non-radiative recombination. In addition, the morphology investigations indicated that *m*-ITIC mainly located on the interface between polymer and fullerene domains, which promoted the bridging effect of *m*-ITIC.

3.3 Enhanced stability

Previous experimental results have suggested that fullerene based OSCs commonly exhibit significant efficiency losses of 25–50% after several hours' light exposure.[75] It has been proposed that the thermally induced fullerene aggregation and photo-induced fullerene dimerization are two important reasons for the quick degradation.[76,77] Therefore, using NFAs with better chemical and morphological stability could be promising for improving the device operation life time. Furthermore, very recent results suggest that some NFA based OSCs also show greater resistance to photo-induced electronic trap state formation than fullerene based cells, leading to significantly enhanced stability upon light irradiation.[78] Although the stability investigations of fullerene free OSCs are still at an early stage, these positive results indicate the prospects for using NFAs to construct more stable OSCs.

Recent research indicates that the stability of fullerene free OSCs can be further improved by adding the third component.[79]

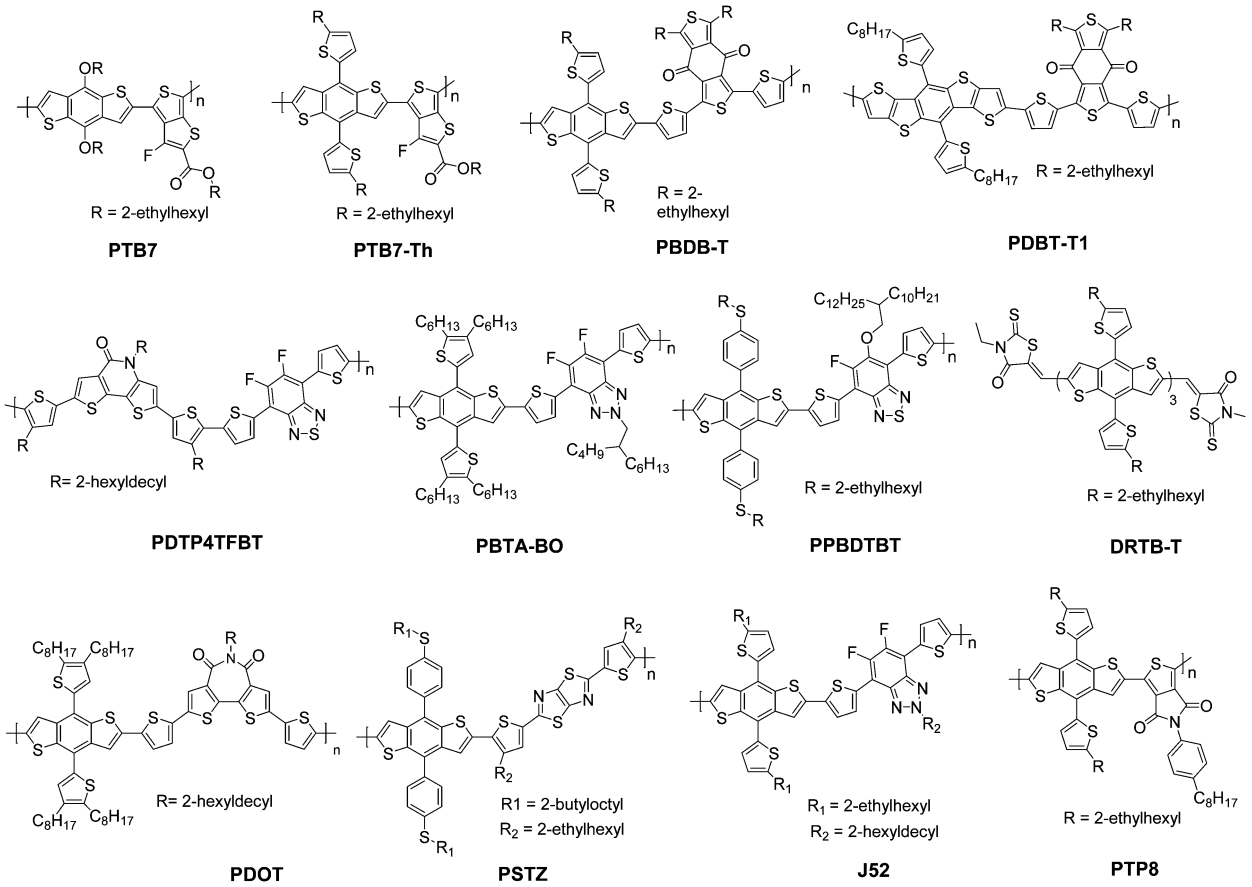

Scheme 3 The molecular structures of donor materials summarized in this review.

Several different material systems, including P3HT:IDTBR:IDFBR (Scheme 2), P3HT:IDTBR, P3HT:IDFBR, P3HT:$PC_{61}BM$, PTB7-Th (PCE10):$PC_{71}BM$ and PCE11:$PC_{71}BM$, were investigated. Both the device storage lifetime and photo-stability under ambient conditions were examined, and the results are shown in Fig. 5. For both the cases, the ternary P3HT : IDTBR : IDFBR (1 : 0.7 : 0.3) OSCs showed the best device stability. In particular, after storing in air and under dark conditions for 1200 h, the optimized P3HT based ternary blend devices retained 80% of their initial PCE values, whereas P3HT:IDTBR binary devices retained 70%. In comparison, all of the fullerene contained devices were no longer operational only after 800 h storage in air. Moreover, for photo-stability tests (un-encapsulated, in air, AM1.5 radiation of 100 mW cm^{-2}), the optimized ternary blend devices presented the best photo-stability as well, retaining 85% of their initial PCE values after 90 h operation. These results demonstrate that the ternary blend approach can improve not only the photovoltaic performance but also the device stability.

Moreover, the other functions of NFAs in ternary OSCs, such as improving the charge separation and transport, providing more flexible energy transfer pathways and options, and improving the film morphology, are also demonstrated in recent research, all of which are discussed with specific examples in the following section.

4. Recent developments in NFA based ternary solar cells

In this section, we summarize the recent progress in developing ternary blend OSCs based on NFAs. Currently, the most popular molecular system for NFAs is a class of calamitic small molecule, which consists of an electron-donating core and two strong electron-withdrawing end cappers. NFAs based on the 2-(3-oxo-2,3-dihydroinden-1-ylidene)malononitrile (IC) electron-withdrawing moiety have been the most efficient material system until now, which have been widely adopted in preparing high performance ternary OSCs.[80–84] The representative molecular structures for the IC family are shown in Scheme 1. Most of these molecules are low band gap materials with an optical band gap (E_g^{opt}) < 1.6 eV, and hence commonly show intense light absorption in the long wavelength range. The rest of the common NFA materials are listed in Scheme 2. Among them, perylene diimide derivatives and naphthalimide based n-type conjugated polymers (*e.g.* N2200) have also been well investigated in ternary cells. Most of them are medium or wide band gap materials (with E_g^{opt} > 1.6 eV), showing intense light absorption in the visible and short wavelength ranges. The common donor materials to match with these NFA materials are depicted in Schemes 3 and 4.

Fig. 6 depicts different possible combinations of ternary OSCs with NFAs. We divide them into two categories, *e.g.* D–2A and 2D–A types.

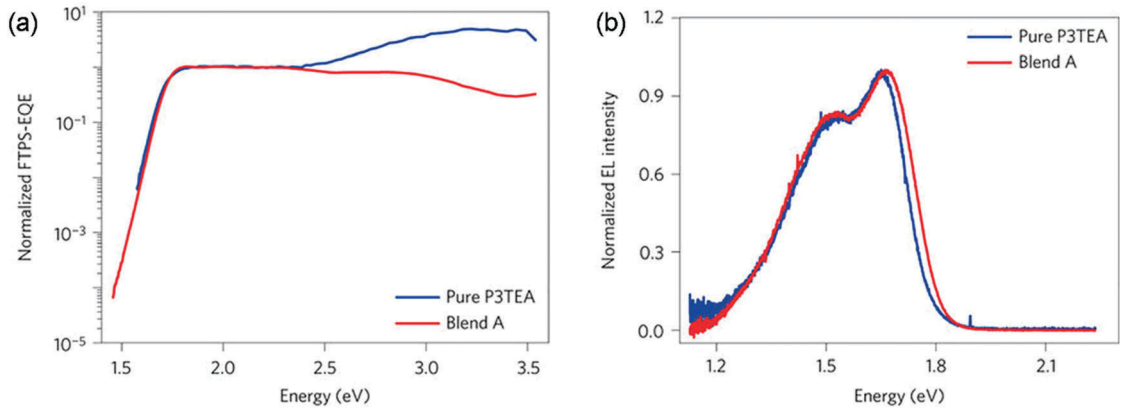

Fig. 4 (a) Normalized Fourier-transform photocurrent spectroscopy external quantum efficiency (FTPS-EQE) spectra of pure P3TEA and P3TEA/SF-PDI (blend A)-based devices. (b) Normalized electroluminescence (EL) curves of pure P3TEA and blend A-based devices. Reproduced with permission.[52] Copyright 2016, Nature Publishing Group.

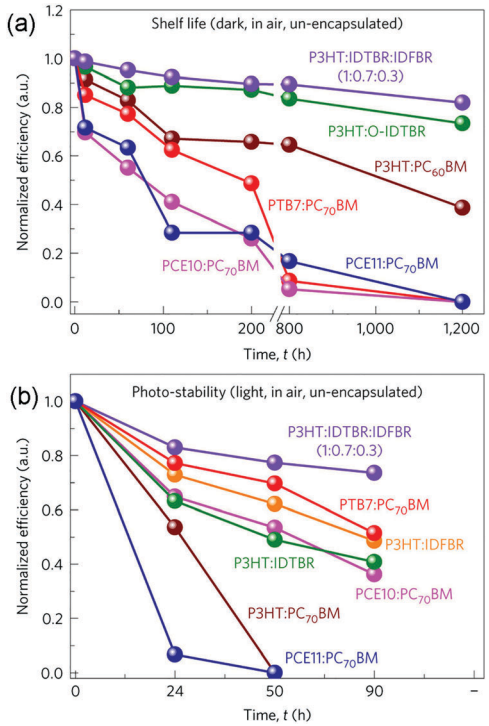

Fig. 5 Storage lifetime (a) and photo-stability (b) tests for various blend compositions. Reproduced with permission.[79] Copyright 2016, Nature Publishing Group.

D–2A type ternary OSCs are further divided into two subcategories, *e.g.* with and without using fullerene. According to the different roles of NFAs in donor/fullerene/NFA blends, they can be classified into another two subcategories that NFAs work as additives for donor/fullerene hosts or work as main light absorbers. Different materials, including p-type polymer/small molecules and n-type polymer/small molecules, can be introduced into ternary blend systems.

4.1 D–2A type ternary OSCs

4.1.1 Donor/fullerene/NFA. According to the feed ratio and role of NFAs in fullerene involved ternary OSCs, their functions can be characterized as an additive for the donor/fullerene host or as the main component. In spite of serious shortcomings, fullerene derivatives also have lots of merits, such as high electron mobility, large electron affinity and isotropic charge transport. It has been demonstrated that introducing a small amount of NFAs into polymer/fullerene blends can help in improving the light absorption, optimizing the morphology and achieving energy level alignment for facilitating charge separation, transport and collection (Table 1).[77,85–88] Some reports suggest that the additional NFA additive in polymer/fullerene blends can even improve the device stability.[89]

Considering the insufficient light harvesting ability of polymer/fullerene binary blend films, introducing a small amount of NFA into a binary host can improve the overall light harvesting ability. For example, the high performance PTB7-Th/$PC_{71}BM$ blend shows relatively weak absorption in the wavelength range around 450–620 nm. Introducing a medium band gap NFA, such as RTCN (Scheme 2), can effectively complement the absorption band, and hence lead to photocurrent enhancement.[86] In addition, for host systems with medium or large band gap polymers, low band gap NFAs (such as ITIC) are favourable for improving the light harvesting ability in the long wavelength range. For instance, adding a small amount of ITIC into PDOT (Scheme 3)/$PC_{71}BM$ blends achieved an extended EQE response in the 650–800 nm region, leading to significantly enhanced J_{SC} and PCE values.[87] Similar improvements in J_{SC} and the EQE response were also observed in PDTP4TFBT (Scheme 3)/$PC_{71}BM$ and PBTA-BO/$PC_{71}BM$ hosts after low band gap NFA loading.[85,90,91]

Furthermore, NFA additives can be utilized to tune the morphology and nanostructure of polymer/fullerene blends. It was reported that a minimal amount of TPE-4PDI (Scheme 2) added (3 wt%) into PTB7-Th:$PC_{71}BM$ leads to an overall enhancement of photovoltaic parameters.[88] Obviously, such a small amount of NFA loading can hardly improve the light harvesting ability. The morphology measurements indicated the formation of an acceptor alloy and a favourable nano-scaled interpenetrating network, helping in improving charge generation and collection and reducing charge recombination. In addition,

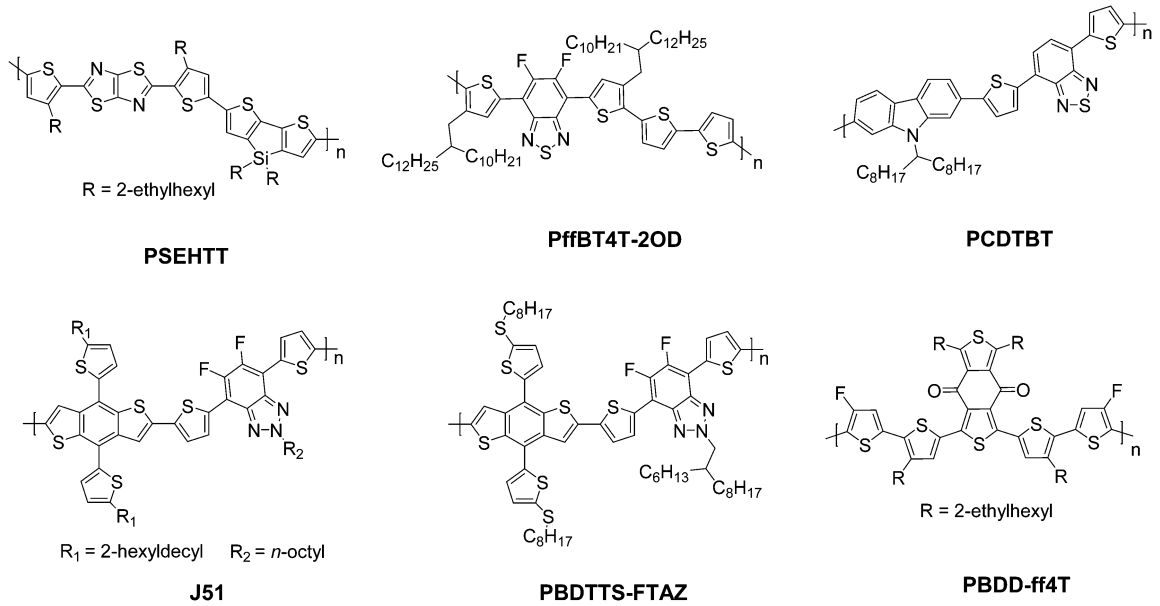

Scheme 4 The molecular structures of donor materials utilized in 2D–A ternary OSCs.

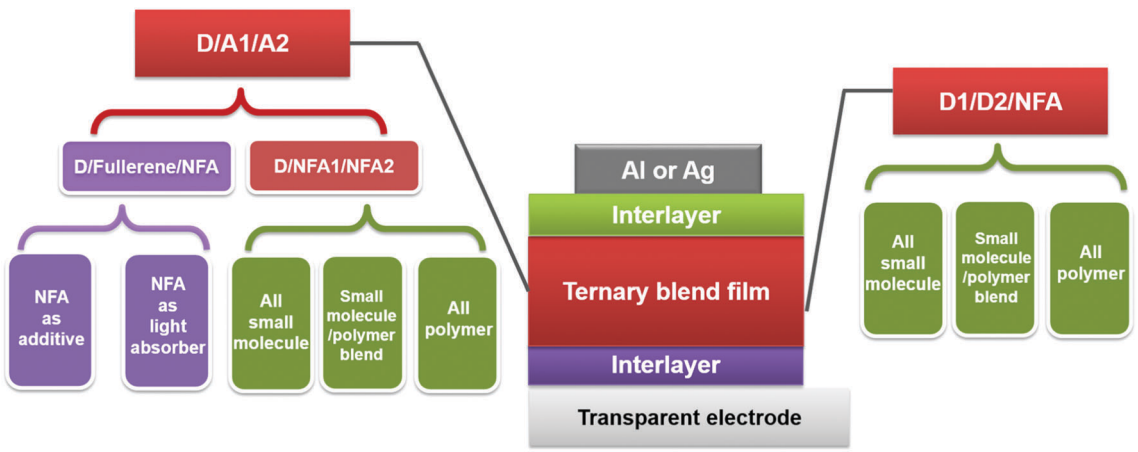

Fig. 6 The illustration of different ternary blend systems.

PBTA-BO/fullerene binary films commonly show a very rugged surface morphology and large aggregation, resulting in inefficient exciton dissociation and transport. To address this issue, two different types of NFAs, namely IFBR and IffBR (Scheme 2), were introduced to construct ternary solar cells.[90,91] In both cases, smooth and favourable phase separated films were formed, leading to significantly improved photovoltaic performance.

In addition to small molecule acceptors, an n-type conjugated polymer (PNDI2OD-T2, Scheme 2) was introduced into a polymer/fullerene blend as an additive.[89] A small amount of PNDI2OD-T2 added (0.8 wt%) into PTB7:$PC_{71}BM$ or PTB7-Th:$PC_{71}BM$ enhanced the photovoltaic performance, which resulted from the improved charge transport and collection. Interestingly, although the macromolecule additive addition did not affect the morphology and molecular packing for pristine films, as suggested by grazing-incidence wide-angle X-ray diffraction (GIWAX) measurements, it did improve the OSC device stability. As shown in Fig. 7, after 10 min annealing at 120 °C in an inert atmosphere, the optimized ternary blend devices retained over 80% of its initialized PCE value. In comparison, a sharp decrease in PCE (50%) was found in the binary control devices. GIWAX examinations demonstrated that the diffraction intensity for PNDI2OD-T2 based ternary blends hardly changed upon heating, but diffraction in either out-of-plane or in-plane directions decreased a lot in binary blend films, indicating the function of PNDI2OD-T2 in stabilizing the polymer/fullerene film morphology and hence the stability.

Very recently, more and more attention has been paid towards developing ternary systems with NFAs as host materials due to their superior performance to fullerene, providing higher starting points for constructing more efficient cells. Hou *et al.*[92] reported a high performance ternary OSC based PBDB-T (Scheme 3)/IT-M (Scheme 1) binary host, which gave a starting point as high as 10.8%. Based on the binary cells with such high efficiency, a more

Table 1 Photovoltaic performances of ternary organic solar cells with donor/fullerene/non-fullerene acceptor blends

				Photovoltaic parameters						
Donor	A1 (fullerene)	A2 (NFA)	Weight ratio (D : A1 : A2)	V_{OC}	J_{SC}	FF (%)	PCE (%)	Binary PCE (D:A1)	Binary PCE (D:A2)	Ref.
PTB7-Th	PC71BM	COi8DFIC	1 : 0.45 : 1.05	0.70	28.20	71.0	14.08	7.36	10.48	45
PTB7-Th	PC71BM	*m*-ITIC	1 : 1.05 : 0.45	0.845	16.1	59.2	8.04	7.52	5.49	74
PBDB-T	PC71BM	BDCPDT-IC	1 : 0.67 : 1	0.84	16.84	68.79	9.73	—	9.33	84
PDTP4TFBT	PC71BM	ITIC	1 : 1.2 : 0.3	0.84	15.82	69.3	9.2	8.75	7.58	85
PTB7-Th	PC71BM	RTCN	1 : 1.5 : 0.2	0.789	17.27	68.9	9.39	8.5	3.9	86
PDOT	PC71BM	ITIC	1 : 1.8 : 0.2	0.96	17.49	66.8	11.21	9.54	5.90	87
PTB7-Th	PC71BM	TPE-4PDI	66.7 : 97 : 3	0.78	17.44	73.9	10.09	9.22	1.88	88
PTB7	PC71BM	P(NDI2OD-T2)	37.2 : 62 : 0.8	0.75	19.2	65	9.97	7.42	—	89
PBTA-BO	PC61BM	IFBR	1 : 1 : 0.8	0.926	13.45	65.07	8.11	5.70	3.85	90
PBTA-BO	PC71BM	IffBR	1 : 1 : 0.6	0.932	14.03	64.69	8.45	4.68	6.24	91
PBDB-T	Bis[70]PCBM	IT-M	1 : 0.2 : 1	0.952	17.39	73.7	12.2	—	10.80	92
PPBDTBT	PC71BM	ITIC	1 : 0.8 : 1.2	0.894	16.66	68	10.35	7.09	7.66	93
PTB7-Th	PC71BM	IEICO	1 : 0.06 : 1.14	0.80	16.67	64	8.61	6.21	8.33	94
PTB7-Th	Bis[70]PCBM	IEICO	1 : 0.06 : 1.14	0.83	18.92	65	10.21	3.5	8.33	94
PTB7-Th	IC70BM	IEICO	1 : 0.06 : 1.14	0.83	18.86	65	10.17	1.73	8.33	94
PDBT-T1	PC71BM	ITIC-Th	1 : 0.5 : 0.5	0.934	15.54	70.5	10.22	9.23	7.05	95
DRTB-T	PC71BM	IDIC	1 : 0.5 : 0.5	0.99	15.36	67.0	10.31	6.04	8.79	96

impressive performance can be expected for ternary cells by rational composition engineering. Since both PBDB-T and IT-M show very weak light absorption in the short wavelength range, fullerene derivatives appear to be good candidates to complement their absorption band. A bis-adduct of phenyl-C70-butyric-acid–methyl ester (Bis-PC70BM) was selected as the additive, and a champion device with a PCE reaching 12.20% was achieved at the optimized feed ratio (PBDB-T : IT-M : Bis[70]PCBM = 1 : 1 : 0.2). EQE measurements confirmed an enhancement of the EQE response in the short wavelength region from 380 nm to 480 nm. Interestingly, it also led to an increased response beyond 550 nm, which indicated that the charge generation from the PBDB-T/IT-M interface also improved after Bis-PC70BM loading.

With a similar motivation for improving the absorption in the short wavelength region, Ding and co-workers reported a record PCE for ternary OSCs by adding a small amount of $PC_{71}BM$ into PTB7-Th:CO_i8DFIC (Scheme 1) blends.[45] The binary host gave a PCE of 10.48% as the starting point. By varying the composition of $PC_{71}BM$, the J_{SC} and FF increased dramatically.

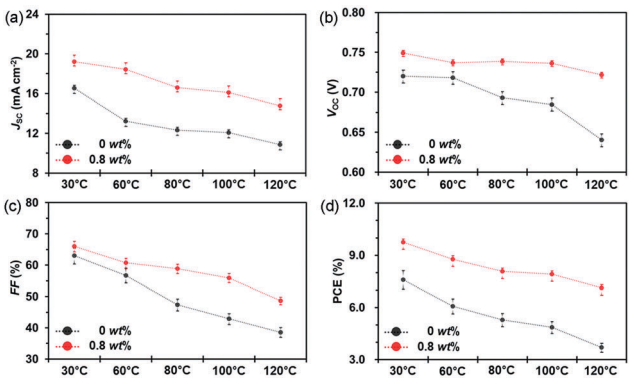

Fig. 7 Device stability of PTB7:$PC_{71}BM$ based OSCs without and with the PNDI2OD-T2 additive (0.8 wt%) exposed to different temperatures (30, 60, 80, 100, and 120 °C): (a) J_{SC}; (b) V_{OC}; (c) FF; and (d) PCE. Reproduced with permission.[89] Copyright 2016, Royal Society of Chemistry.

The champion device showed a large J_{SC} of 28.20 mA cm^{-2}, a V_{OC} of 0.70 V, and an FF of 71.0, giving a high PCE of 14.08% (Fig. 8c). Fig. 8a and d exhibit UV-Vis-NIR absorption of the active materials and EQE spectra for the binary and ternary solar cells, respectively. Compared with its major binary counterparts, the ternary device showed a stronger EQE response at 310–550 and 864–1050 nm, which originated from $PC_{71}BM$ and CO_i8DFIC absorption, respectively. The dramatically enhanced EQE response in the short wavelength region indicates an improvement in charge generation and transport. Further investigation suggested that the $PC_{71}BM$ addition balanced charge carrier transport, reduced charge recombination and improved the film morphology.

For high performance polymer/NFA hosts, by judiciously selecting the energy level of the third component, such as designing a cascade energy level alignment, it is possible to further improve charge separation and hence device performance. This strategy was first demonstrated in fullerene involved systems, where PPBDTBT (Scheme 3) was used as the donor and ITIC and $PC_{71}BM$ were used as the acceptors.[93] There were additional charge transfer processes that occurred at the PPBDTBT/ITIC and ITIC/$PC_{71}BM$ interfaces due to the existence of an energy level offset. Here ITIC worked as a bridge for extracting electrons from PPBDTBT and delivering charges to $PC_{71}BM$. Within such a cascade charge transfer, a significantly enhanced PCE of up to 10.41% was achieved, which was almost 35% enhancement relative to the binary devices. Another excellent result was achieved in a NFA rich system (PTB7-Th/IEICO) host, in which a minute amount of fullerene (5wt% ICBA or Bis-PC70BM) addition resulted in boosted PCE values due to the introduction of cascade-like charge transfer pathways.[94]

Most of the recent morphological investigations on polymer/fullerene/NFA blends have indicated the formation of an acceptor alloy when the feed ratio of the third component is low. The optimized alloy phase commonly provides a more suitable scaled donor/acceptor interpenetrating network, which effectively improves charge separation and transport and reduces recombination. However, most of the cases have also suggested

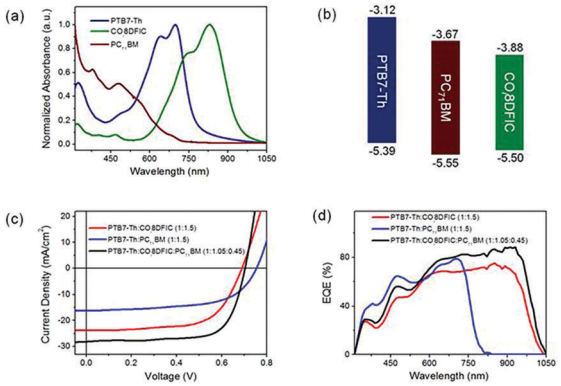

Fig. 8 (a) Absorption spectra for PTB7-Th, COi8DFIC and PC71BM films. (b) Energy level diagrams. (c) *J*–*V* curves for the binary and ternary solar cells. (d) EQE spectra for the binary and ternary solar cells.[45] Copyright 2017, Elsevier.

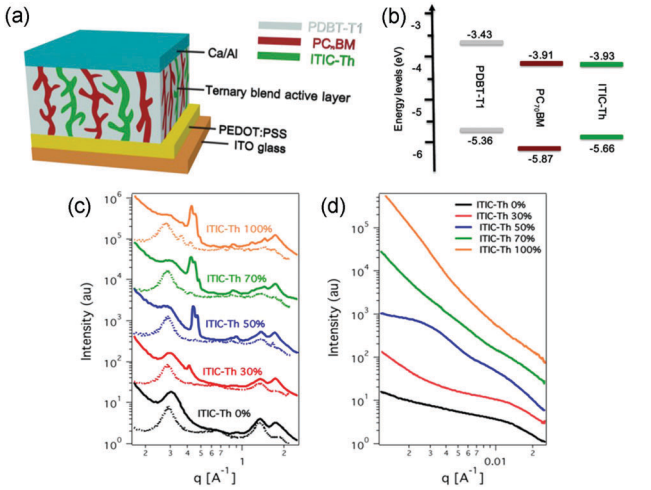

Fig. 9 (a) An illustration for ternary OSC devices with parallel-like blends. (b) The energy level for the donor (PDBT-T1) and acceptors (ITIC-Th and $PC_{71}BM$). (c) Out of plane (solid line) and in plane (dotted line) line cut profiles of GIWAX results of ITIC-Th:$PC_{71}BM$ blend films with different ITIC-Th contents. (d) RSoXS profiles of ITIC-Th:$PC_{71}BM$ blend films with different ITIC-Th contents. Reproduced with permission.[95] Copyright 2017, American Chemical Society.

that a strong phase separated film morphology can be observed upon increasing the feed ratio of the third component, which commonly results in an efficiency drop and strong composition dependent performance.[74,86,88] We assume that it originates from the distinguished molecular topology and crystalline orientation for fullerene and NFAs. The strong crystallinity and the tendency of aggregations of widely utilized planar NFAs can also be important reasons.

A parallel-like model has also been observed in the polymer/fullerene/NFA system. It was first demonstrated in a ternary system with blends of PDBT-T1 (Scheme 3), $PC_{71}BM$ and ITIC-Th.[95] The photophysical studies suggested that there was no charge transfer or energy transfer between ITIC-Th and $PC_{71}BM$. In particular, the PL intensity of ITIC-Th was independent of the $PC_{71}BM$ content in mixed thin films. There was also very little variation in the PL decay of ITIC-Th and ITIC-Th/$PC_{71}BM$ films. This phenomenon can be attributed to the negligible LUMO offset between ITIC-Th and $PC_{71}BM$, as illustrated in Fig. 10a. The parallel-like morphological feature was confirmed by GIWAX and RSoXS studies. As shown in Fig. 9c, when the ITIC-Th content was more than 30%, diffraction peaks for all the components, including PDBT-T1 feature domains (out of plane, q = 0.3 Å^{-1}), ITIC-Th domains (out of plane, q = 0.41 Å^{-1}), and $PC_{71}BM$ domains (out of plane, q = 1.35 Å^{-1}), appeared, demonstrating that all the components could form their own domains in the blend films. The reflections in the out of plane direction indicated a face-on orientation for all the phases. For RSoXS measurements (Fig. 9d), PDBT-T1:$PC_{71}BM$ blends showed a shoulder in the scattering at 0.014 Å^{-1}, corresponding to a length scale of 45 nm for its phase-separated domain. The RSoXS profile showed two shoulders in the scattering at 0.013 Å^{-1} (48 nm) and 0.003 Å^{-1} (210 nm), indicating a multi-length scale morphology, for a sample with 50% ITIC-Th content, which happened to be the optimized feed ratio for device performance. The device with 50% ITIC-Th content gave the highest PCE of 10.48%. All these results demonstrated that the two electron acceptors worked independently in the ternary blend films.

4.1.2 Donor/NFA1/NFA2. For high performance polymer/NFA systems, by further composition engineering through the rational introduction of another NFA, more efficient OSCs can be achieved. Compared to donor/fullerene/NFA blends, a fullerene free system shows much better flexibility for composition modification, and hence provides numerous opportunities to improve the device performance. It has been well demonstrated in the past year, and lots of encouraging results have been presented (Table 2).

From the viewpoint of improving the light harvesting ability of the active layer, a very popular material combination strategy in recent reports is to construct ternary blend films with a low band gap IC based NFA and a perylene diimide or naphthalene diimide derivative with a medium band gap. Such mixtures show clear advantages to achieve a broad band absorption. Various kinds of acceptor systems, such as ITIC/EP-PDI, ITIC-Th/TPE-4PDI, ITIC/P(NDI2HD-T), and ITIC-Th/SdiPBI-Se, have been explored.[97–100] All of these material systems demonstrated an enhancement in the J_{SC} and EQE response.

The versatile chemical structures of NFAs can provide flexible choices to design cascade charge transfer pathways for more efficient charge separation and transport, in addition to the benefits for improving light absorption as mentioned above. It was demonstrated in a recent report using PTB7-Th/IDT-2BR (Scheme 2) as the host system.[101] The host materials show a small energy level offset around 0.1 eV, resulting in a large V_{OC} of up to 1.05 V and a good starting point of 8.2% PCE. PDI-2DTT (Scheme 2), whose energy level was deeper than both of the host materials, was selected as the third component. With only 1 wt% PDI-2DTT addition, both the J_{SC} and FF increased significantly. The third component worked as an energy driver to enhance the driving force for exciton dissociation, and the low feed ratio

Table 2 Photovoltaic performances of ternary organic solar cells with two different non-fullerene acceptors

				Photovoltaic parameters						
D	A1	A2	Ratio (D : A1 : A2)	V_{OC}	J_{SC}	FF (%)	PCE (%)	Binary PCE (D : A1)	Binary PCE (D : A2)	Ref.
P3HT	IDTBR	IDFBR	1 : 0.7 : 0.3	0.82	14.4	64	7.7	6.3	—	79
PTB7-Th	IDTBR	IDFBR	1 : 0.5 : 0.5	1.03	17.2	60	11.0	—	—	79
PTB7-Th	ITIC	EP-PDI	1 : 1.4 : 0.6	0.84	18.37	56.0	8.64	7.51	3.7	97
PBDB-T	ITIC-Th	TPE-4PDI	1 : 0.9 : 0.1	0.87	17.2	72.6	10.82	9.75	4.73	98
PTP8	P(NDI2HD-T)	ITIC	1.5 : 0.85 : 0.15	0.976	12.60	57	7.01	6.00	5.10	99
PBDB-T1	SdiPBI-Se	ITIC-Th	1 : 0.5 : 0.5	0.931	15.37	70.2	10.1	8.12	6.39	100
PTB7-Th	IDT-2BR	PDI-2DTT	1 : 1 : 0.02	1.03	14.5	65.0	9.7	8.2	—	101
PSTZ	ITIC	IDIC	1 : 0.1 : 0.9	0.953	17.40	66.9	11.1	8.13	8.06	104
J52	IT-M	IEICO	1 : 0.8 : 0.2	0.847	19.7	66.8	11.1	9.4	6.5	105
P3HT	*p*-DPP-PhCN	*o*-DPP-PhCN	1 : 0.75 : 0.25	0.99	2.04	49	1.00	0.47	—	106
PBDTTT-CT	PNDIS-HD	PPDIS	1 : 0.25 : 0.75	0.745	9.43	44	3.16	1.33	2.09	122

ensured its negligible effect on reducing V_{OC}. Therefore, it leads to significant photovoltaic performance improvement.

It is observed that most of the recently developed high performance NFAs, such as the IC family and perylene diimide derivatives, tend to form large aggregates and result in a strong phase separated film due to their planar molecular topology and strong crystallinity.[48,102,103] It leads to a reduced donor/acceptor interfacial area and strong recombination loss, which significantly limits the further improvement of device performance.

Here we highlight a facile approach to overcome the morphological issues of state-of-the-art fullerene free binary OSCs using two well miscible acceptors together (alloy-like model), which has been well demonstrated by several groups in succession. It was first proposed in a ternary system including both a perylene diimide derivative (SdiPBI-Se, Scheme 2) and an IC-family material (ITIC-Th, Scheme 1).[100] In this case, PDBT-T1 (Scheme 3) was utilized as the electron donor. The GIWAX studies suggested that SdiPBI-Se and ITIC-Th were miscible, and a new mixing phase with reduced crystallinity formed in ternary blend films. The molecular dynamics simulations confirmed that there was a strong tendency of molecular binding between ITIC-Th and SdiPBI-Se. Transmission electron microscopy (TEM) characterization gave a distinctive morphological picture for morphological variation. As shown in Fig. 10, both PDBT-T1:SdiPBI-Se (Fig. 10a and d) and PDBT-T1:ITIC-Th binary blends (Fig. 10c and f) showed large aggregates and strong phase separation. However, in the ternary mixture (Fig. 10b and e), the acceptor aggregation was suppressed and a more favorable nano-scaled interpenetrating network was formed. The formation of the new acceptor phase with a suitable domain size facilitated the charge generation and transport. By varying the compositions, the champion cell showed the highest PCE value of 10.3%, significantly outperforming its binary PDBT-T1:ITIC-Th (8.15%) and PDBT-T1:SdiPBI-Se counterparts (6.43%).

The excellent compatibility of two NFAs is critical for the new acceptor phase formation and morphology optimization, which can be simply achieved by selecting NFAs with similar molecular structures. This idea was proposed in two recent ternary systems with ITIC/IDIC and IT-M/IEICO as acceptors.[104,105] In both cases, the good material compatibility led to the formation of a new acceptor alloy and much more continuous films.

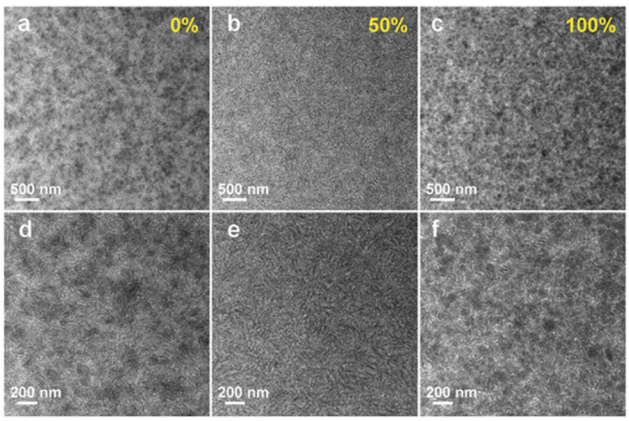

Fig. 10 TEM images of blend films: (a and d) PDBT-T1:SdiPBI-Se film, (b and e) PDBT-T1:SdiPBI-Se film with 50% ITIC-Th, and (c and f) PDBT-T1:ITIC-Th film. The scale bars for (a–c) are 500 nm and for (d–f) are 200 nm. Reproduced with permission.[100] Copyright 2016, Wiley.

This implied successful inhibition of aggregate formation. Therefore, boosted PCE values were achieved. In addition, in IT-M/IEICO based ternary OSCs, the good overlap between the PL spectrum of IT-M and the absorption band of IEICO resulted in an efficient energy transfer process. This suggests that the fullerene free ternary blend approach provides much more flexible energy transfer channels than fullerene involved systems, and there is no doubt that it is promising for designing more efficient ternary OSCs.

4.2 2D-NFA type ternary OSCs

As mentioned above, currently high performance IC moiety based NFAs are a series of low band gap materials, and their light absorption in the short wavelength region is poor. Even for the most efficient NFA based binary OSCs, the utilization of high energy solar photons (400–550 nm) is insufficient.[45,50,80,92] Besides exploring high performance wide band gap polymer donors which can match well with the absorption band of high performance NFAs, investigations on 2D-NFA type ternary OSCs can be a simple method to further improve the light harvesting ability of the active layer.[107,108] However, there are few research activities towards this research direction compared to D–2A systems (Table 3).

Table 3 Photovoltaic performances of ternary organic solar cells with two donors and one non-fullerene acceptor

				Photovoltaic parameters						
D1	D2	NFA	Ratio (D1 : D2 : NFA)	V_{OC}	J_{SC}	FF (%)	PCE (%)	Binary PCE (D1:A)	Binary PCE (D2:A)	Ref.
J52	PTB7-Th	IEICO-4F	0.3 : 0.7 : 1.5	0.731	25.3	58.9	10.9	9.4	10.0	50
PSEHTT	PTB7-Th	DBFI-EDOT	0.9 : 0.1 : 2	0.91	15.67	60.0	8.52	8.10	6.70	107
PTB7-Th	PffBT4T-2OD	ITIC	0.8 : 0.2 : 1.5	0.84	15.36	62.6	8.05	6.35	4.42	108
PTB7-Th	PCDTBT	ITIC	0.8 : 0.2 : 1.3	0.80	16.71	55.91	7.51	6.51	—	111
J51	PTB7-Th	ITIC	0.8 : 0.2 : 1	0.81	17.75	67.82	9.70	8.89	6.56	112
PTB7-Th	PBDD-ff4T	N2200	1.25 : 0.25 : 1	0.82	15.7	56	7.2	5.9	4.2	118
PTB7-Th	PBDTTS-FTAZ	PNDI-T10	1 : 0.15 : 1	0.84	14.4	74	9.0	7.6	6.0	119
PTB7-Th	PCDTBT	N2200	0.8 : 0.2 : 1	0.78	11.44	56	5.11	4.23	0.96	120
PTB7-Th	PCDTBT	N2200	1 : 0.11 : 1	0.79	14.4	58.3	6.65	5.70	0.77	121

Introducing a FRET process by adding a wide band gap polymer is an effective way to improve solar energy utilization, especially for the light in the short wavelength region.[109,110] For 2D-NFA ternary OSCs, an interesting report reveals that efficient energy transfer possibly occurs between all three components. PCDTBT has been well investigated in previous ternary OSCs as an energy donor. It was introduced into PTB7-Th:ITIC blends to improve the light harvesting of the active layer.[111] The emission of PCDTBT was found to strongly overlap with the absorption bands of both PTB7-Th and ITIC, as shown in Fig. 11a. This indicated that the possible existence of FRET between both PCDTBT/PTB7-Th and PCDTBT/ITIC. This was further verified by the enhanced steady state PL intensities of PTB7-Th and ITIC in their 20 wt% PCDTBT blended films with respect to their neat films (Fig. 11b), as well as the significantly decreased PL lifetime. Consequently, in contrast to the control device showing a PCE value of 6.51%, a higher PCE reaching 7.51% was achieved in the ternary counterparts with optimized feed ratios. Moreover, a more efficient 2D–A ternary blend system was constructed with the blends of J51 (Scheme 4)/PTB7-Th/ITIC.[112] In this case, an energy transfer process occurred from J51 to PTB7-Th. Together with other benefits, such as improving the morphology and balancing charge carrier transport, an optimized PCE value of up to 9.70% was achieved.

Developing all-polymer solar cells (APSCs) have recently attracted considerable attention due to their potential advantages, especially for their excellent morphology stability and mechanical durability.[113–115] Although there have been several reports on high performance APSCs with PCE > 9%, the value is still much lower than their polymer/fullerene and polymer/small molecule NFA counterparts.[116,117] N2200 and its derivatives are the most widely utilized polymer acceptors due to their broad light absorption, good electron affinity and high mobility. However, their morphological problematic features, such as large aggregate formation, strong phase separation, and inhomogeneous internal phase composition, result in strong charge recombination. In addition, insufficient coverage of the solar spectrum is still problematic in binary blend APSCs.

The ternary blend approach appears to be a promising way to improve the efficiency of APSCs. The general advantages of ternary OSCs, such as enhancing the solar energy utilization, reducing the charge transfer barrier through the cascade energy level, and improving the film morphology, are also demonstrated

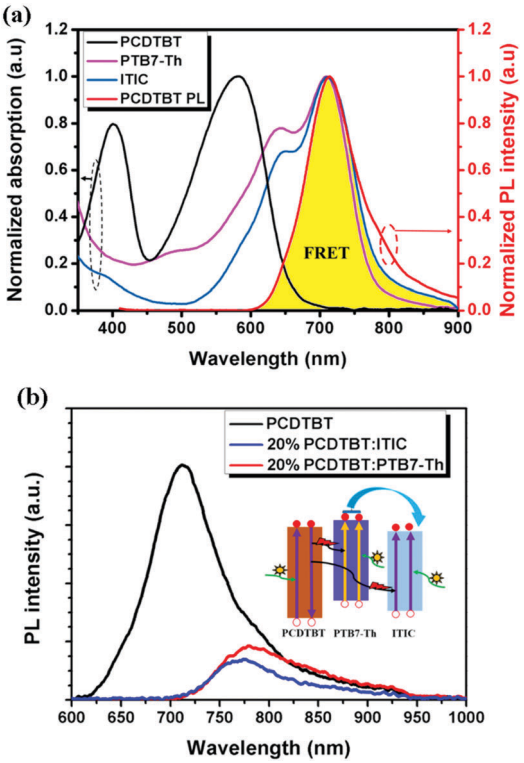

Fig. 11 (a) Normalized UV-Vis absorption spectra of PTB7-Th, ITIC, and PCDTBT films and the normalized PL spectrum of the PCDTBT film. (b) PL spectra of a neat PCDTBT film, a 20 wt% PCDTBT:PTB7-Th film and a 20 wt% PCDTBT:ITIC film with an excitation wavelength of 500 nm (inset: diagram showing the dual FRET effects for energy transfer from PCDTBT to PTB7-Th and ITIC). Reproduced with permission.[111] Copyright 2017, Royal Society of Chemistry.

in ternary APSCs.[118–121] Although there have also been some attempts to prepare D–2A type ternary APSCs, the lack of efficient polymer acceptors currently limits their performance.[122] In addition, some NIR sensitizers have also been incorporated. Unfortunately, the poor performance of host materials resulted in very limited efficiency improvement.[123] A more reasonable and popular strategy in the current stage is to prepare 2D–A type ternary APSCs, and the light absorption enhancement can be simply achieved by incorporating another p-type light absorber. A large band gap polymer, PCDTBT, was first introduced into PTB7-Th/P(NDI2OD-T2) polymer blends to increase the utilization of

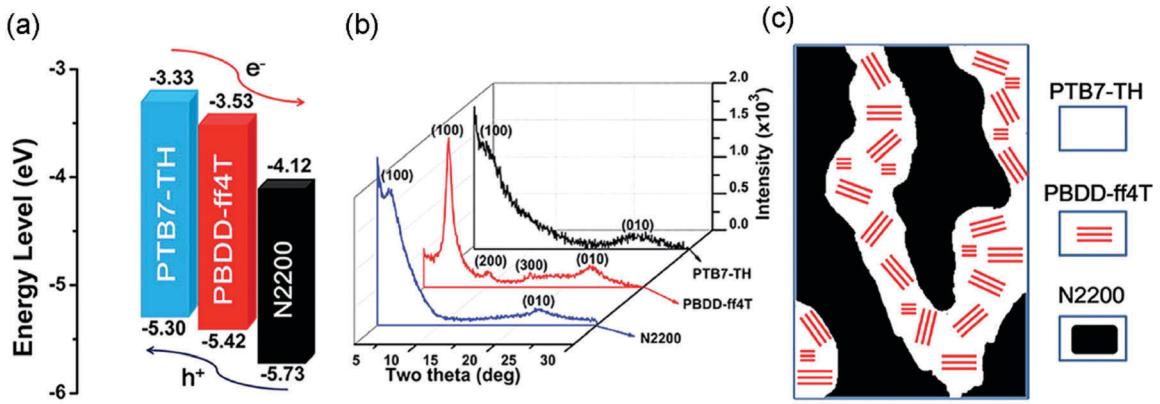

Fig. 12 (a) Electronic energy levels of the three polymers; (b) XRD patterns of the pure polymer films; and (c) schematic diagram of the donor/acceptor interpenetrating network showing crystalline PBDD-ff4T embedded in PTB7-Th. Reproduced with permission.[118] Copyright 2016, Royal Society of Chemistry.

solar photons in the short wavelength region through a FRET process.[121,123] This resulted in a significantly enhanced J_{SC} and hence the PCE value.

A particular challenging issue of state-of-the-art APSCs is the lack of efficient methods to optimize phase separated polymer/polymer blend films. Li *et al.* reported the introduction of a highly crystalline polymer donor, PBDD-ff4T (Scheme 4), into PTB7-Th:N2200 blends.[118] PBDD-ff4T tended to fully embed into the PTB7-Th phase to form a donor alloy, which induced the crystallization of PTB7-Th, as depicted in Fig. 12b and c. By varying the content of PBDD-ff4T, an optimized bi-continuous interpenetrating network with suitable domain size and crystallinity was achieved. Together with the benefits of the cascade energy level, as suggested in Fig. 12a, the ternary device champion exhibited a PCE of 7.2%, which was much higher than that of the control device (5.9%). This work demonstrates that the morphology of APSCs can be finely tuned by adding the third polymer component, and it is very promising for future developments of preparing more efficient APSCs.

The progress in exploring more efficient n-type conjugated polymers can provide high starting points for preparing ternary APSCs. A naphthalimide based random co-polymer, named PNDI-T10 (Scheme 2), was designed and synthesized.[119] It features reduced backbone rigidity and crystallinity with respect to the widely utilized N2200.[124] For the ternary blends, a large band gap polymer, namely PBDTTS-FTAZ (Scheme 4), was introduced into PTB7-Th/PNDI-T10 to enhance the light absorption in the short wavelength region, resulting in J_{SC} enhancement and a high PCE value of over 9%.

5. Summary and perspectives

It is clear that the emergence of high performance NFAs provides flexible options to rationally design and construct high performance ternary blend OSCs. The small voltage loss and excellent light absorbing ability of NFAs provide a high starting point for developing more efficient ternary OSCs. In the past two years, it has become one of the hottest research topics in OSC research fields due to the combination of the most efficient materials and advanced device optimization strategies. Though promising, there are still several challenges to be noted and addressed.

A breakthrough in materials development always triggers a rapid growth of device performance in OSCs. In the past several years, a wide range of NFAs has been developed. However, NFAs with certified efficiencies exceeding 10% in binary OSCs are still limited, especially for polymer acceptors. It is notable that an ITIC like polymer was developed very recently, which achieved a high efficiency of over 9% in all-polymer blend systems.[115] It provides a new idea for developing novel efficient polymer acceptors in addition to the N2200 family, and their future applications in ternary OSCs are also promising. For donor materials, previous investigations mainly focused on developing low band gap polymers due to the poor light absorbing ability of fullerene. In fact, most of the high performance NFAs show strong absorption in the long wavelength region (700–950 nm). Therefore, there is an urgent requirement for developing high performance medium band gap or wide band gap donor materials to match their energy level and complement their absorption band.

Further explorations of material combinations have the potential to achieve better device performance. For example, small molecule donor (SMD) materials commonly offer distinct advantages over their conjugated polymer counterparts, such as well-defined molecular structures, high purity and fewer defects. Promising results have been reported with polymer/small molecule/fullerene ternary blends.[33] However, research on all small molecule fullerene free ternary blends is rare. The remarkable results achieved in recent reports on developing SMD/small molecule acceptor (SMA) and SMD/SMA/fullerene based OSCs indicate their advantages and prospects.[96,125] In addition, optimizing the morphologies of all-polymer solar cells is particularly challenging, which has become the key issue limiting the development of all-polymer solar cells. The ternary blend approach appears to be a powerful tool to tune

the molecular packing, phase aggregation and domain size, which provides a good opportunity to finely tune the film morphology of all-polymer films. Other advantages, such as improving light harvesting and facilitating exciton dissociation and charge transport, are also attractive.

It has been suggested that NFA based OSCs show better photo-stability, thermal stability and storage stability compared to fullerene derivatives.[78] However, achieving their long-term operational stability is still a big challenge. In addition to improving molecular stability on heat and light illumination through molecular designing, the morphological stability is equally important. Although there have been several successful attempts within the ternary approach towards this direction,[79,89] future investigations are certainly needed to further enhance the stability and understand the mechanisms.

A power conversion efficiency as high as 15% is commonly regarded as the target for enabling commercial viability. Considering a starting point as high as 13% achieved in fullerene free binary blend OSCs, the combination of high performance non-fullerene acceptors and the ternary blend strategy provides bright prospects for pushing the performance of OSCs to the stage of commercial applications.

Conflicts of interest

There are no conflicts to declare.

Acknowledgements

The authors acknowledge financial support from the Wenner-Gren Foundation (UPD2016-0144), the Swedish Research Council VR (Grant No. 2017-00744), the Swedish Energy Agency – Energimyndigheten (2016-010174), the Swedish Government Strategic Research Area in Materials Science on Functional Materials at Linköping University (Faculty Grant No. SFO-Mat-LiU #2009-00971), the National Natural Science Foundation of China (61704077), the Natural Science Foundation of Jiangsu Province (BK20171007), and the China Postdoctoral Science Foundation (2016M601784, 2017T100358).

Notes and references

1 A. Polman, M. Knight, E. C. Garnett, B. Ehrler and W. C. Sinke, *Science*, 2016, **352**, aad4424.
2 S. Zhang, L. Ye and J. Hou, *Adv. Energy Mater.*, 2016, **6**, 1502529.
3 A. J. Heeger, *Adv. Mater.*, 2014, **26**, 10–28.
4 H. Kang, G. Kim, J. Kim, S. Kwon, H. Kim and K. Lee, *Adv. Mater.*, 2016, **28**, 7821–7861.
5 B. Azzopardi, C. J. M. Emmott, A. Urbina, F. C. Krebs, J. Mutale and J. Nelson, *Energy Environ. Sci.*, 2011, **4**, 3741–3753.
6 L. Lu, T. Zheng, Q. Wu, A. M. Schneider, D. Zhao and L. Yu, *Chem. Rev.*, 2015, **115**, 12666–12731.
7 Z. Yin, J. Wei and Q. Zheng, *Adv. Sci.*, 2016, **3**, 1500362.
8 M. C. Scharber and N. S. Sariciftci, *Prog. Polym. Sci.*, 2013, **38**, 1929–1940.
9 B. Maennig, J. Drechsel, D. Gebeyehu, P. Simon, F. Kozlowski, A. Werner, F. Li, S. Grundmann, S. Sonntag, M. Koch, K. Leo, M. Pfeiffer, H. Hoppe, D. Meissner, N. S. Sariciftci, I. Riedel, V. Dyakonov and J. Parisi, *Appl. Phys. A: Mater. Sci. Process.*, 2004, **79**, 1–14.
10 C. J. Brabec, N. S. Sariciftci and J. C. Hummelen, *Adv. Funct. Mater.*, 2001, **11**, 15–26.
11 S. Günes, H. Neugebauer and N. S. Sariciftci, *Chem. Rev.*, 2007, **107**, 1324–1338.
12 C. Deibel and V. Dyakonov, *Rep. Prog. Phys.*, 2010, **73**, 096401.
13 H. Hoppe and N. S. Sariciftci, *J. Mater. Res.*, 2004, **19**, 1924–1945.
14 C. R. McNeill and N. C. Greenham, *Adv. Mater.*, 2009, **21**, 3840–3850.
15 M. M. Koetse, J. Sweelssen, K. T. Hoekerd, H. F. M. Schoo, S. C. Veenstra, J. M. Kroon, X. Yang and J. Loos, *Appl. Phys. Lett.*, 2006, **88**, 88–91.
16 E. Zimmermann, P. Ehrenreich, T. Pfadler, J. A. Dorman, J. Weickert and L. Schmidt-Mende, *Nat. Photonics*, 2014, **8**, 669–672.
17 F. Gao and O. Inganäs, *Phys. Chem. Chem. Phys.*, 2014, **16**, 20291–20304.
18 J. Weickert, R. B. Dunbar, H. C. Hesse, W. Wiedemann and L. Schmidt-Mende, *Adv. Mater.*, 2011, **23**, 1810–1828.
19 W. Wiedemann, L. Sims, A. Abdellah, A. Exner, R. Meier, K. P. Musselman, J. L. MacManus-Driscoll, P. Müller-Buschbaum, G. Scarpa, P. Lugli and L. Schmidt-Mende, *Appl. Phys. Lett.*, 2010, **96**, 78–81.
20 S. Guo, J. Ning, V. Körstgens, Y. Yao, E. M. Herzig, S. V. Roth and P. Müller-Buschbaum, *Adv. Energy Mater.*, 2015, **5**, 1401315.
21 M. A. Ruderer, S. Guo, R. Meier, H. Y. Chiang, V. Körstgens, J. Wiedersich, J. Perlich, S. V. Roth and P. Müller-Buschbaum, *Adv. Funct. Mater.*, 2011, **21**, 3382–3391.
22 P. Müller-Buschbaum, *Adv. Mater.*, 2014, **26**, 7692–7709.
23 X. Yang, J. Loos, S. C. Veenstra, W. J. H. Verhees, M. M. Wienk, J. M. Kroon, M. A. J. Michels and R. A. J. Janssen, *Nano Lett.*, 2005, **5**, 579–583.
24 X. Yang and J. Loos, *Macromolecules*, 2007, **40**, 1353–1362.
25 T. Ameri, G. Dennler, C. Lungenschmied and C. J. Brabec, *Energy Environ. Sci.*, 2009, **2**, 347–363.
26 J. You, L. Dou, Z. Hong, G. Li and Y. Yang, *Prog. Polym. Sci.*, 2013, **38**, 1909–1928.
27 T. Ameri, N. Li and C. J. Brabec, *Energy Environ. Sci.*, 2013, **6**, 2390–2413.
28 H. Lu, X. Xu and Z. Bo, *Sci. China Mater.*, 2016, **59**, 444–458.
29 P. Cheng and X. Zhan, *Mater. Horiz.*, 2015, **2**, 462–485.
30 Q. An, F. Zhang, J. Zhang, W. Tang, Z. Deng and B. Hu, *Energy Environ. Sci.*, 2016, **9**, 281–322.
31 Y. C. Chen, C. Y. Hsu, R. Y. Y. Lin, K. C. Ho and J. T. Lin, *ChemSusChem*, 2013, **6**, 20–35.
32 T. Ameri, P. Khoram, J. Min and C. J. Brabec, *Adv. Mater.*, 2013, **25**, 4245–4266.

33 H. Li, K. Lu and Z. Wei, *Adv. Energy Mater.*, 2016, **7**, 1602540.
34 L. Lu, M. A. Kelly, W. You and L. Yu, *Nat. Photonics*, 2015, **9**, 491–500.
35 L. Lu, T. Xu, W. Chen, E. S. Landry and L. Yu, *Nat. Photonics*, 2014, **8**, 716–722.
36 L. Lu, W. Chen, T. Xu and L. Yu, *Nat. Commun.*, 2015, **6**, 7327.
37 N. Gasparini, L. Lucera, M. Salvador, M. Prosa, G. D. Spyropoulos, P. Kubis, H.-J. Egelhaaf, C. J. Brabec and T. Ameri, *Energy Environ. Sci.*, 2017, **10**, 885–892.
38 L. Nian, K. Gao, F. Liu, Y. Kan, X. Jiang, L. Liu, Z. Xie, X. Peng, T. P. Russell and Y. Ma, *Adv. Mater.*, 2016, **28**, 8184–8190.
39 J. Zhang, Y. Zhang, J. Fang, K. Lu, Z. Wang, W. Ma and Z. Wei, *J. Am. Chem. Soc.*, 2015, **137**, 8176–8183.
40 S. Li, W. Liu, C.-Z. Li, M. Shi and H. Chen, *Small*, 2017, **13**, 1701120.
41 C. B. Nielsen, S. Holliday, H.-Y. Chen, S. J. Cryer and I. McCulloch, *Acc. Chem. Res.*, 2015, **48**, 2803–2812.
42 J. H. Hou, O. Inganäs, R. H. Friend and F. Gao, *Nat. Mater.*, 2018, **17**, 119–128.
43 W. Zhao, S. Li, H. Yao, S. Zhang, Y. Zhang, B. Yang and J. Hou, *J. Am. Chem. Soc.*, 2017, **139**, 7148–7151.
44 H. Huang, L. Yang and B. Sharma, *J. Mater. Chem. A*, 2017, **5**, 11501–11517.
45 Z. Xiao, X. Jia and L. Ding, *Sci. Bull.*, 2017, **62**, 1562–1564.
46 L. Yang, L. Yan and W. You, *J. Phys. Chem. Lett.*, 2013, **4**, 1802–1810.
47 L. Zhang and W. Ma, *Chin. J. Polym. Sci.*, 2017, **35**, 184–197.
48 J. Zhao, Y. Li, H. Lin, Y. Liu, K. Jiang, C. Mu, T. Ma, J. Y. L. Lai, H. Hu, D. Yu and H. Yan, *Energy Environ. Sci.*, 2015, **8**, 520–525.
49 H. Yao, Y. Chen, Y. Qin, R. Yu, Y. Cui, B. Yang, S. Li, K. Zhang and J. Hou, *Adv. Mater.*, 2016, **28**, 8283–8287.
50 H. Yao, Y. Cui, R. Yu, B. Gao, H. Zhang and J. Hou, *Angew. Chem., Int. Ed.*, 2017, **56**, 3045–3049.
51 Y. Lin, J. Wang, Z.-G. Zhang, H. Bai, Y. Li, D. Zhu and X. Zhan, *Adv. Mater.*, 2015, **27**, 1170–1174.
52 J. Liu, S. Chen, D. Qian, B. Gautam, G. Yang, J. Zhao, J. Bergqvist, F. Zhang, W. Ma, H. Ade, O. Inganäs, K. Gundogdu, F. Gao and H. Yan, *Nat. Energy*, 2016, **1**, 16089.
53 K. Vandewal, K. Tvingstedt, A. Gadisa, O. Inganäs and J. V. Manca, *Nat. Mater.*, 2009, **8**, 904–909.
54 J. Yao, T. Kirchartz, M. S. Vezie, M. A. Faist, W. Gong, Z. He, H. Wu, J. Troughton, T. Watson, D. Bryant and J. Nelson, *Phys. Rev. Appl.*, 2015, **4**, 014020.
55 C. M. Ramsdale, J. A. Barker, A. C. Arias, J. D. MacKenzie, R. H. Friend and N. C. Greenham, *J. Appl. Phys.*, 2002, **92**, 4266–4270.
56 S. Westenhoff, *J. Am. Chem. Soc.*, 2008, **130**, 13653–13658.
57 C. Deibel, T. Strobel and V. Dyakonov, *Phys. Rev. Lett.*, 2009, **103**, 036402.
58 C. Deibe, T. Strobe and V. Dyakonov, *Adv. Mater.*, 2010, **22**, 4097–4111.
59 M. Saliba, T. Matsui, K. Domanski, J.-Y. Seo, A. Ummadisingu, S. M. Zakeeruddin, J.-P. Correa-Baena, W. R. Tress, A. Abate, A. Hagfeldt and M. Gratzel, *Science*, 2016, **354**, 206–209.
60 C. Battaglia, A. Cuevas and S. De Wolf, *Energy Environ. Sci.*, 2016, **9**, 1552–1576.
61 W. Yang, Y. Yao and C. Q. Wu, *J. Appl. Phys.*, 2015, **117**, 095502.
62 M. Wang, H. Wang, T. Yokoyama, X. Liu, Y. Huang, Y. Zhang, T. Q. Nguyen, S. Aramaki and G. C. Bazan, *J. Am. Chem. Soc.*, 2014, **136**, 12576–12579.
63 K. Vandewal, Z. Ma, J. Bergqvist, Z. Tang, E. Wang, P. Henriksson, K. Tvingstedt, M. R. Andersson and F. Zhang, *Adv. Funct. Mater.*, 2012, **22**, 3480–3490.
64 N. A. Ran, J. A. Love, C. J. Takacs, A. Sadhanala, J. K. Beavers, S. D. Collins, Y. Huang, M. Wang, R. H. Friend, G. C. Bazan and T. Q. Nguyen, *Adv. Mater.*, 2016, **28**, 1482–1488.
65 W. Li, K. H. Hendriks, A. Furlan, M. M. Wienk and R. A. J. Janssen, *J. Am. Chem. Soc.*, 2015, **137**, 2231–2234.
66 K. Kawashima, Y. Tamai, H. Ohkita, I. Osaka and K. Takimiya, *Nat. Commun.*, 2015, **6**, 10085.
67 Z. Ma, E. Wang, K. Vandewal, M. R. Andersson and F. Zhang, *Appl. Phys. Lett.*, 2011, **99**, 143302.
68 K. Vandewal, K. Tvingstedt, A. Gadisa, O. Inganäs and J. V. Manca, *Phys. Rev. B: Condens. Matter Mater. Phys.*, 2010, **81**, 125204.
69 D. Baran, T. Kirchartz, S. Wheeler, S. Dimitrov, M. Abdelsamie, J. Gorman, R. S. Ashraf, S. Holliday, A. Wadsworth, N. Gasparini, P. Kaienburg, H. Yan, A. Amassian, C. J. Brabec, J. R. Durrant and I. McCulloch, *Energy Environ. Sci.*, 2016, **9**, 3783–3793.
70 P. P. Khlyabich, B. Burkhart and B. C. Thompson, *J. Am. Chem. Soc.*, 2011, **133**, 14534–14537.
71 P. P. Khlyabich, B. Burkhart and B. C. Thompson, *J. Am. Chem. Soc.*, 2012, **134**, 9074–9077.
72 B. M. Savoie, S. Dunaisky, T. J. Marks and M. A. Ratner, *Adv. Energy Mater.*, 2015, **5**, 1400891.
73 R. A. Street, D. Davies, P. P. Khlyabich, B. Burkhart and B. C. Thompson, *J. Am. Chem. Soc.*, 2013, **135**, 986–989.
74 C. Wang, X. Xu, W. Zhang, S. Ben Dkhil, X. Meng, X. Liu, O. Margeat, A. Yartsev, W. Ma, J. Ackermann, E. Wang and M. Fahlman, *Nano Energy*, 2017, **37**, 24–31.
75 R. Roesch, K. R. Eberhardt, S. Engmann, G. Gobsch and H. Hoppe, *Sol. Energy Mater. Sol. Cells*, 2013, **117**, 59–66.
76 K. P. Meletov, J. Arvanitidis, D. Christofilos, G. A. Kourouklis and V. A. Davydov, *Chem. Phys. Lett.*, 2016, **654**, 81–85.
77 H. C. Wong, Z. Li, C. H. Tan, H. Zhong, Z. Huang, H. Bronstein, I. McCulloch, J. T. Cabral and J. R. Durrant, *ACS Nano*, 2014, **8**, 1297–1308.
78 H. Cha, J. Wu, A. Wadsworth, J. Nagitta, S. Limbu, S. Pont, Z. Li, J. Searle, M. F. Wyatt, D. Baran, J. S. Kim, I. McCulloch and J. R. Durrant, *Adv. Mater.*, 2017, **29**, 1701156.
79 D. Baran, R. S. Ashraf, D. A. Hanifi, M. Abdelsamie, N. Gasparini, J. A. Röhr, S. Holliday, A. Wadsworth, S. Lockett, M. Neophytou, C. J. M. Emmott, J. Nelson, C. J. Brabec, A. Amassian, A. Salleo, T. Kirchartz, J. R. Durrant and I. McCulloch, *Nat. Mater.*, 2016, **16**, 363–369.

80 W. Zhao, D. Qian, S. Zhang, S. Li, O. Inganäs, F. Gao and J. Hou, *Adv. Mater.*, 2016, **28**, 4734–4739.
81 Y. Lin, F. Zhao, Q. He, L. Huo, Y. Wu, T. C. Parker, W. Ma, Y. Sun, C. Wang, D. Zhu, A. J. Heeger, S. R. Marder and X. Zhan, *J. Am. Chem. Soc.*, 2016, **138**, 4955–4961.
82 L. Yang, S. Zhang, C. He, J. Zhang, H. Yao, Y. Yang, Y. Zhang, W. Zhao and J. Hou, *J. Am. Chem. Soc.*, 2017, **139**, 1958–1966.
83 S. Li, L. Ye, W. Zhao, S. Zhang, H. Ade and J. Hou, *Adv. Energy Mater.*, 2017, **7**, 1700183.
84 S. L. Chang, F. Y. Cao, W. C. Huang, P. K. Huang, C. S. Hsu and Y. J. Cheng, *ACS Appl. Mater. Interfaces*, 2017, **9**, 24797–24803.
85 M. An, F. Xie, X. Geng, J. Zhang, J. Jiang, Z. Lei, D. He, Z. Xiao and L. Ding, *Adv. Energy Mater.*, 2017, **7**, 1602509.
86 Y. Wang, W.-D. Xu, J.-D. Zhang, L. Zhou, G. Lei, C.-F. Liu, W.-Y. Lai and W. Huang, *J. Mater. Chem. A*, 2017, **5**, 2460–2465.
87 T. Zhang, X. Zhao, D. Yang, Y. Tian and X. Yang, *Adv. Energy Mater.*, 2017, **7**, 1701691.
88 Y. Chen, P. Ye, Z.-G. Zhu, X. Wang, L. Yang, X. Z. Xu, X. X. Xu, T. Dong, H. Zhang, J. Hou, F. Liu and H. Huang, *Adv. Mater.*, 2017, **29**, 1603154.
89 K. H. Park, Y. An, S. Jung, H. Park and C. Yang, *Energy Environ. Sci.*, 2016, **9**, 3464–3471.
90 B. Fan, W. Zhong, X. F. Jiang, Q. Yin, L. Ying, F. Huang and Y. Cao, *Adv. Energy Mater.*, 2017, **7**, 1602127.
91 W. Zhong, J. Cui, B. Fan, L. Ying, Y. Wang, G. Zhang, X. Jiang, F. Huang and Y. Cao, *Chem. Mater.*, 2017, **29**, 8177–8186.
92 W. Zhao, S. Li, S. Zhang, X. Liu and J. Hou, *Adv. Mater.*, 2017, **29**, 1604059.
93 H. Lu, J. Zhang, J. Chen, Q. Liu, X. Gong, S. Feng, X. Xu, W. Ma and Z. Bo, *Adv. Mater.*, 2017, **28**, 9559–9566.
94 Y. Chen, Y. Qin, Y. Wu, C. Li, H. Yao, N. Liang, X. Wang, W. Li, W. Ma and J. Hou, *Adv. Energy Mater.*, 2017, **7**, 1700328.
95 T. Liu, X. Xue, L. Huo, X. Sun, Q. An, F. Zhang, T. P. Russell, F. Liu and Y. Sun, *Chem. Mater.*, 2017, **29**, 2914–2920.
96 H. Zhang, X. Wang, L. Yang, S. Zhang, Y. Zhang, C. He, W. Ma and J. Hou, *Adv. Mater.*, 2017, **13**, 1703777.
97 J. Wang, J. Peng, X. Liu and Z. Liang, *ACS Appl. Mater. Interfaces*, 2017, **9**, 20704–20710.
98 Y. Chen, P. Ye, X. Jia, W. Gu, X. Xu, X. Wu, J. Wu, F. Liu, Z.-G. Zhu and H. Huang, *J. Mater. Chem. A*, 2017, **5**, 19697–19702.
99 G. Ding, J. Yuan, F. Jin, Y. Zhang, L. Han, X. Ling, H. Zhao and W. Ma, *Nano Energy*, 2017, **36**, 356–362.
100 T. Liu, Y. Guo, Y. Yi, L. Huo, X. Xue, X. Sun, H. Fu, W. Xiong, D. Meng, Z. Wang, F. Liu, T. P. Russell and Y. Sun, *Adv. Mater.*, 2016, **28**, 10008–10015.
101 P. Cheng, M. Zhang, T. K. Lau, Y. Wu, B. Jia, J. Wang, C. Yan, M. Qin, X. Lu and X. Zhan, *Adv. Mater.*, 2017, **29**, 1605216.
102 D. Sun, D. Meng, Y. Cai, B. Fan, Y. Li, W. Jiang, L. Huo, Y. Sun and Z. Wang, *J. Am. Chem. Soc.*, 2015, **137**, 11156–11162.
103 D. Meng, D. Sun, C. Zhong, T. Liu, B. Fan, L. Huo, Y. Li, W. Jiang, H. Choi, T. Kim, J. Y. Kim, Y. Sun, Z. Wang and A. J. Heeger, *J. Am. Chem. Soc.*, 2016, **138**, 375–380.
104 W. Su, Q. Fan, X. Guo, X. Meng, Z. Bi, W. Ma, M. Zhang and Y. Li, *Nano Energy*, 2017, **38**, 510–517.
105 R. Yu, S. Zhang, H. Yao, B. Guo, S. Li, H. Zhang, M. Zhang and J. Hou, *Adv. Mater.*, 2017, **29**, 1700437.
106 Y. Kim, C. E. Song, E.-J. Ko, D. Kim, S.-J. Moon and E. Lim, *RSC Adv.*, 2014, **5**, 4811–4821.
107 Y. J. Hwang, H. Li, B. A. E. Courtright, S. Subramaniyan and S. A. Jenekhe, *Adv. Mater.*, 2016, **28**, 124–131.
108 X. Liu, J. Wang, J. Peng and Z. Liang, *Macromolecules*, 2017, **50**, 6954–6960.
109 V. Gupta, V. Bharti, M. Kumar, S. Chand and A. J. Heeger, *Adv. Mater.*, 2015, **27**, 4398–4404.
110 P. C. Dastoor, *Nat. Photonics*, 2013, **7**, 425–426.
111 P.-Q. Bi, F. Zheng, X.-Y. Yang, M.-S. Niu, L. Feng, W. Qin and X. Hao, *J. Mater. Chem. A*, 2017, **5**, 12120–12130.
112 L. Zhong, L. Gao, H. Bin, Q. Hu, Z. G. Zhang, F. Liu, T. P. Russell, Z. Zhang and Y. Li, *Adv. Energy Mater.*, 2017, **7**, 1602215.
113 H. Kang, W. Lee, J. Oh, T. Kim, C. Lee and B. J. Kim, *Acc. Chem. Res.*, 2016, **49**, 2424–2434.
114 H. Benten, D. Mori, H. Ohkita and S. Ito, *J. Mater. Chem. A*, 2016, **4**, 5340–5365.
115 A. Facchetti, *Mater. Today*, 2013, **16**, 123–132.
116 Y. Li, Z.-G. Zhang, Y. Yang, J. Yao, L. Xue, S. Chen, X. Li, W. Morrison and C. Yang, *Angew. Chem., Int. Ed.*, 2017, **56**, 13503–13507.
117 B. Fan, L. Ying, Z. Wang, B. He, X.-F. Jiang, F. Huang and Y. Cao, *Energy Environ. Sci.*, 2017, **10**, 1243–1251.
118 W. Su, Q. Fan, X. Guo, B. Guo, W. Li, Y. Zhang, M. Zhang and Y. Li, *J. Mater. Chem. A*, 2016, **4**, 14752–14760.
119 Z. Li, X. Xu, W. Zhang, X. Meng, Z. Genene, W. Ma, W. Mammo, A. Yartsev, M. R. Andersson, R. A. J. Janssen and E. Wang, *Energy Environ. Sci.*, 2017, **10**, 2212–2221.
120 R. Zhang, H. Yang, K. Zhou, J. Zhang, J. Liu, X. Yu, R. Xing and Y. Han, *J. Polym. Sci., Part B: Polym. Phys.*, 2016, **54**, 1811–1819.
121 H. Benten, T. Nishida, D. Mori, H. Xu, H. Ohkita and S. Ito, *Energy Environ. Sci.*, 2016, **9**, 135–140.
122 Y.-J. Hwang, B. A. E. Courtright and S. A. Jenekhe, *MRS Commun.*, 2015, **5**, 229–234.
123 H. Xu, H. Ohkita, T. Hirata, H. Benten and S. Ito, *Polymer*, 2014, **55**, 2856–2860.
124 Z. Li, X. Xu, W. Zhang, X. Meng, W. Ma, A. Yartsev, O. Inganäs, M. R. Andersson, R. A. J. Janssen and E. Wang, *J. Am. Chem. Soc.*, 2016, **138**, 10935–10944.
125 H. Bin, Y. Yang, Z. G. Zhang, L. Ye, M. Ghasemi, S. Chen, Y. Zhang, C. Zhang, C. Sun, L. Xue, C. Yang, H. Ade and Y. Li, *J. Am. Chem. Soc.*, 2017, **139**, 5085–5094.